Title

Steps to achieving high-resolution NMR spectroscopy on solutions at GPa pressure

Journal

American Journal of Science, 317(7)

ISSN

0002-9599

Authors

Augustine, Matthew P
Ochoa, Gerardo
Casey, William H

Publication Date

2017-09-01

DOI

10.2475/07.2017.03

Peer reviewed

[American Journal of Science, Vol. 317, September, 2017, P. 845–859, DOI 10.2475/07.2017.03]

STEPS TO ACHIEVING HIGH-RESOLUTION NMR SPECTROSCOPY ON SOLUTIONS AT GPa PRESSURE

MATTHEW P. AUGUSTINE*, GERARDO OCHOA*, and WILLIAM H. CASEY*,**,†

ABSTRACT. Recent theoretical advances and molecular-dynamic estimates of the dielectric constant of water have extended the HKF model for aqueous solution chemistry up to 6.0 gigapascals (GPa), which are conditions well beyond the capabilities of conventional NMR spectroscopy (Pan and others, 2013; Sverjensky and others, 2014, see also Wasserman and others, 1995). These developments provide strong motivation to design a simple NMR probe that allows experiments on solutions, at high resolution, to pressures of a few GPa (Pautler and others, 2014; Ochoa and others, 2015, 2016). Here we describe the performance of a compact NMR probe that can reach several GPa pressures. The probe is made by placing a solenoid microcoil inside of a standard piston-cylinder device used in solid-state physics. High pressures are achieved in the sample by applying force to a coaxial piston. Early designs of the probe, although useful, were limited in sample size to ~10 to 15 μL. Here we describe modifications that allow greatly improved resolution and sensitivity, including ^{1}H-^{1}H NMR correlation spectroscopy, on solutions at 2.8 GPa pressure.

Sample sizes can be expanded if, instead of a standard NMR spectrometer that is built around a superconducting magnet, one employs a magnetic-resonance imaging (MRI) system that is built around a permanent magnet. The MRI systems can apply larger magnetic field gradients than conventional spectrometers, and thus have more robust shimming capability, which is needed because of the juxtaposition of different alloys in the pressure cell. More importantly, these systems can have magnetic fields that are oriented perpendicular to the magnet bore, which allows rotation of the coil within the axis of the pressure cell to increase sample volumes and pressure. Sensitivity is improved by replacing the traditional, but reduced-volume, *closed* sample container mounted in the center of the NMR detection coil with an *open* NMR coil that dangles freely in solution, thus making the sample solution itself the pressure-transmission fluid. The efficacy of these modifications are demonstrated by measuring ^{1}H NMR spectra for ethyl alcohol and ethyl alcohol/methyl alcohol mixtures at pressures up to 2.8 GPa. Further developments are discussed that will allow geochemists to acquire aqueous solution NMR spectra at higher 3 to 4 GPa pressures.

Key words: spectroscopy, aqueous geochemistry, high-pressure experimentation, solution geochemistry, aqueous speciation

INTRODUCTION

Geochemists are interested in the properties of aqueous solutions at high pressures and temperatures because these fluids modify the Earth's crust. Consequently they have constructed theoretical models to describe the thermodynamic properties of electrolyte solutions up to 6.0 GPa and 1200 °C (Pan and others, 2013; Sverjensky and others, 2014, 2015). Nuclear magnetic resonance (NMR) is an ideal tool for verifying these theoretical predictions because a spectrum directly provides information about aqueous speciation and dynamics, and would complement vibrational and optical spectroscopic measurements (for example, Facq and others, 2014, 2016). High-pressure NMR spectroscopy is, of course, also a familiar tool in inorganic solution chemistry (Asano and Noble, 1978; Van Eldik and others, 1989; Drljaca and others, 1998), but the pressures are less than ≈0.4 GPa, save for a few ambitious exceptions

* Department of Chemistry, University of California Davis, 1 Shields Avenue, California 95616 (USA)
** Department of Earth and Planetary Sciences, University of California Davis, 1 Shields Avenue, Davis, California 95616 (USA)
† Corresponding author: whcasey@ucdavis.edu

where solute NMR spectra at pressures up to ≈0.9 GPa in milliliter-volume aqueous solutions are reported (Jonas, 1980; Lang and Ludemann, 1993; De Langen and Prins, 1995; Ballard and others, 1998). Although diamond-anvil cell (DAC) technology can reach higher pressures, the samples are nanoliter or picoliter volumes (for example, Lee and others, 1987; Meier and others, 2015), which are inadequate for detecting solutes in aqueous solutions via NMR.

Developments that promise to extend this pressure range to a few GPa are described here. The pressure range for aqueous solution NMR was recently pushed to ≈2.0 GPa by placing the NMR detection coil inside of a familiar piston-cylinder device, called a clamped cell, which is commonly used by the high-pressure solid-state physics community (for example, Walker, 1999). Relevant parts of the resulting NMR probe are portrayed in figure 1A and this geometry was used to obtain ^{11}B NMR signals from aqueous borate complexes up to 1.2 GPa (Pautler and others, 2014) and ^{139}La NMR signals up to 1.9 GPa (Ochoa and others, 2015, 2016). In this design, a closed PEEK© (polyether ether ketone) tube holds ≈10–15 μL of sample (fig. 1A) and is surrounded by a pressure-transmission oil held in a deformable Delrin® capsule. The capsule is housed in a 6.3-mm confining cylinder and is strained by opposing tungsten-carbide rods. This ≈2.0 GPa pressure limit can be doubled if technical barriers in the current design are overcome, as discussed below.

Design changes to achieve higher pressures

The NMR sensitivity in the current ≈2.0 GPa design is limited by the sample size and the coil geometry. In the probe configuration shown in figure 1A, the long axis of the radio frequency (rf) coil is constrained by a standard superconducting magnet to lie perpendicular to the long axis of the clamped-cell piston, which is parallel to both the magnet bore and the magnetic-field axes. Thus the rf coil can be no longer than ≈5 mm without impinging on the wall of the confining cylinder and the sample size is limited. An additional consequence of this geometry is that the surface area of the drive piston cannot be reduced to increase pressure without losing signal.

Access to a permanent-magnet-based magnetic-resonance imaging (MRI) system relieves some of these limitations. For example, the direction of the applied static field in some MRI systems is rotated from an alignment that is parallel to the magnet bore to an alignment that is perpendicular to the magnet bore. The rf coil can be rotated similarly, as illustrated in figure 1B, if the static field is rotated. Rotating the coil (fig. 1A) to be coaxial with the bore of the cylinder (fig. 1B) allows the diameter of the tungsten-carbide rod to be decreased, which allows higher pressures to be achieved from the same external applied force. Immersing the coil in the sample and eliminating the pressure-transmission oil also improves sensitivity, as is discussed below, but this immersion introduces spectral distortions that must be corrected.

A permanent-magnet-based MRI system is also attractive because these systems are typically used in industrial settings and are optimized to provide ppm-wide lines on apple-sized sample volumes. These systems have high-current magnetic-field shims that improve the homogeneity of the magnetic field over the sample. This shimming of the magnetic field to improve homogeneity at the sample is particularly important for high-pressure research because so many materials are employed in the probe that have widely varying magnetic susceptibilities. In a conventional NMR spectrometer, five amps of shim-supply current are typically divided into at least eighteen channels and these divided currents are directed to shim coils that adjust the magnetic field across the sample. However, the shim coils in a conventional spectrometer often cannot compensate for the magnetic-susceptibility artifacts that arise by surrounding a millimeter-sized sample tube (fig. 1) in a high-pressure NMR probe with deforming plastics, exotic alloys and tungsten carbide rods. In contrast, in most MRI instruments there are 100 amp/channel gradient shims available, which allow greater control over the

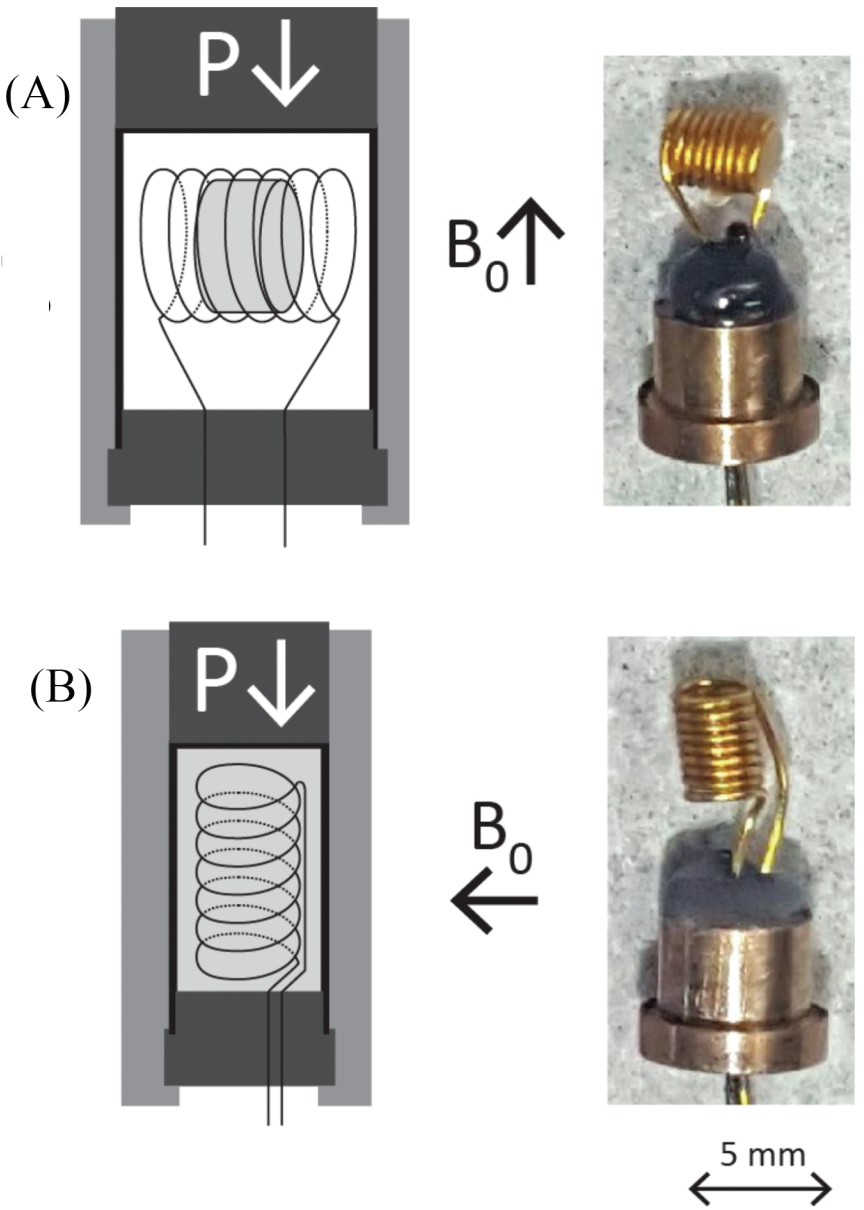

Fig. 1. Coil geometries used in this work where the single arrows indicate the direction of the applied pressure, P, and the static magnetic field B_0. In the *closed* geometry (A), the solenoid coil is oriented perpendicular to the axis of the pressure cylinder and magnet bore. In the *open* geometry (B), the solenoid is rotated to be coaxial to the bore of the piston cylinder and dangled directly into the sample without a sample tube.

magnetic field. Although not normally desired for conventional NMR spectroscopy, the decreased field of the permanent magnet systems (tens of MHz Larmor frequencies instead of hundreds of MHz Larmor frequencies) is also beneficial for acquiring high-resolution spectra because the contributions of the exotic-alloy susceptibility to the observed NMR linewidth are smaller.

Two key adaptations to the probe would allow even higher GPa-pressure NMR spectra to be monitored, including rotation of the solenoid NMR detection coil so that it is coaxial with the piston cylinder and elimination of the sample tube as shown in figure 1B. In this new *open* geometry, ≈0.4 mL of the sample itself serves as the pressure-transmission fluid, allowing higher pressures to be achieved with greater NMR detection sensitivity. However, moving to the *open* geometry makes acquisition of multi-dimensional NMR difficult, as the rf-pulse-excitation efficiency decreases and unwanted spin echoes are produced that corrupt the resulting signals, as is demonstrated below.

The following sections report rf-pulse nutation and three rf-pulse-stimulated-echo results for samples in the standard *closed* geometry in figure 1A and compare these to samples in the new *open* geometry in figure 1B. The primary distortion of generating unwanted spin echoes in multi-pulse interferrograms is resolved by incorporating pulsed magnetic-field gradients, an effort that led to chemically resolved two-dimensional ^{1}H chemical-shift-correlation spectra at 2.8 GPa. These are, to our knowledge, the highest-pressure NMR spectra reported for liquids and are certainly the highest pressure ^{1}H-^{1}H NMR correlation spectra yet achieved.

EXPERIMENTAL DETAILS

Aqueous solutions and most pressure-transmission oils freeze at ambient temperatures and the pressures achieved here. To avoid the complexities of heating and to demonstrate the use of the new probe, the only two samples used in this study were pure ethyl alcohol and a 20% ethyl alcohol/80% deuterated methyl alcohol (volume/volume) solution, which remains liquid to 10 GPa at ambient temperatures (Piermarini and others, 1973). The reagent-grade alcohol solutions were used as received; no further purification was performed to remove residual water from the solutions. The general design of the high-pressure NMR probe is described in earlier papers (Pautler and others, 2014; Ochoa and others, 2015, 2016) and will not be reviewed thoroughly here. Briefly, the probe is built around a Berylco-25 clamped cell and uses a solenoid NMR detection coil made of 28 gauge Berylco-25 wire that resists extrusion at high pressure. In this *closed* geometry shown in figure 1A, the sample is sealed into a cylindrical capsule of PEEK© tubing containing the ≈10–15 μL experimental solution. The cylindrical capsule is sealed at each end with waterproof epoxy, as shown in the photo in the right hand column of figure 1A. The leads for the solenoid NMR detection coil are passed through small holes in the assembly and sealed with a mixture of Stycast© epoxy and a small amount of Al_2O_3 powder. A ruby sphere is attached to a 200 μm diameter fiber-optic cable that is also passed through the feedthrough, positioned just below the solenoid NMR detection coil, and sealed into the vessel. A separate, identically constructed NMR probe head having an identical solenoid for rf transmission and detection, but rotated as in figure 1B and immersed in the ≈0.4 mL sample, serves as the *open* configuration.

Pressure is measured *in situ* using ruby fluorescence where movement of the R1 peak with pressure (Mao and others, 1986; Koyama-Nakazawa and others, 2007) is monitored using an Ocean Optics HR4000 UV-VIS spectrometer. The uncertainties are estimated as ± 30 MPa by propagating a ± 0.01 nm estimated uncertainty in the R1 fluorescence peak position through the equations relating the ruby fluorescence shift to pressure (Dewaele and others, 2008). Uncertainties for the 2.8 GPa experiment are estimated at ± 100 MPa. Pressure for this sample was estimated using a separately measured standard curve that relates hydraulic press force to achieved pressure (fig. 2) as indicated by fluorescence of an immersed ruby sphere. A typical calibration curve is shown in figure 2. Experiments at 2.8 GPa were conducted identically as those at lower pressure, except that the 2.54-cm diameter Berylco-25 confining cylinder was replaced with a 3.81-cm diameter cylinder that was made of stronger MP35N alloy. The internal

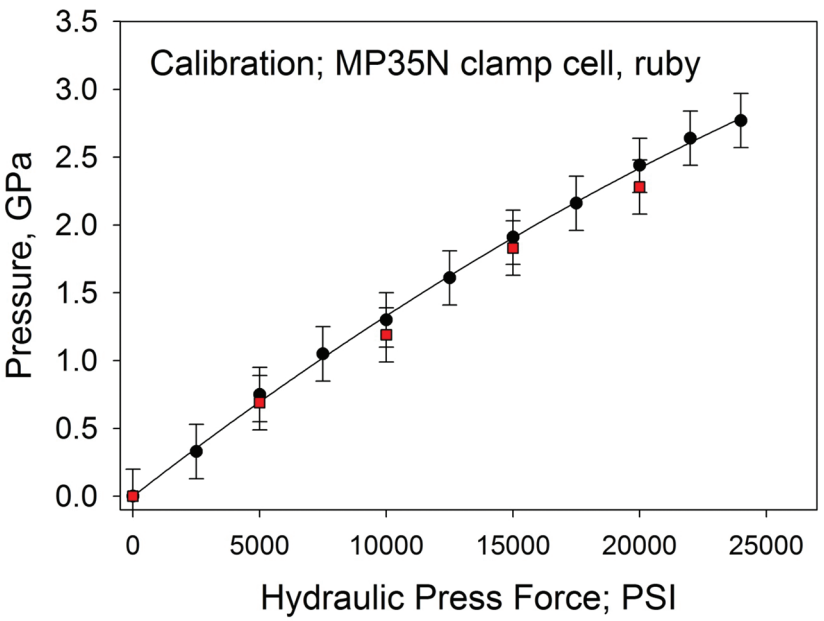

Fig. 2. Two calibration curves between applied pressure (gauge pressure in pounds-per-square inch, abscissa) and the pressure estimated from the fluorescence of the ruby. The cylinder in this case is the same one used to achieve 2.8 GPa NMR spectra (see below) and is fabricated out of MP35N alloy. The red and black symbols indicate two separate trials.

diameter of the channel through these two cylinders was constant at 6.3 mm. Replacement of the cylinder was the only change in the design. For these experiments, the NMR probe is mounted inside of an Aspect Imaging M2 magnet interfaced to a Tecmag Apollo NMR spectrometer. The 1.01 Tesla (43 MHz ^{1}H Larmor frequency) M2 magnet is key to the success of these experiments as the static magnetic field points perpendicular to the long axis of the magnet bore, as described above.

The changes described above also introduce distortions into the NMR signals. Both the distortions, and their resolution, are demonstrated below via three types of experiments: (i) a nutation experiment to show the distortion; (ii) a stimulated-echo experiment to show how the distortions can be surmounted, and finally, (iii) a ^{1}H-^{1}H spin-echo-correlated (SECSY) experiment at 2.8 GPa to show what can be achieved. The pulse sequences for the nutation, three-pulse stimulated-echo, and spin-echo-correlated spectroscopy experiments, respectively, are shown in figures 3A–3C.

In the nutation and stimulated-echo pulse experiments the performance of the traditional *closed* geometry is directly compared with the alternative *open* geometry, where the coil dangles freely in the sample. These two experiments will demonstrate the effects of rf inhomogeneity on single- and multiple-rf-pulse excitation and the distortions that ensue from the geometry changes shown in figure 1.

The distortions are eliminated by pulsed magnetic-field gradients that allow one to edit multiple-pulse transient signals to isolate specific spin echoes. This selection of spin echoes is important because it allows one to obtain SECSY data that can be manipulated offline into two-dimensional ^{1}H chemical-shift-correlation spectra (Nagayama and others, 1979, 1980). In this experiment, a standard value for the $\pi/2$ rf pulse length of 25 μs was always used, while at most 7.5 G/cm, 3-ms-long field-gradient pulses were used for spin-echo selection. All NMR data was processed using Matlab.

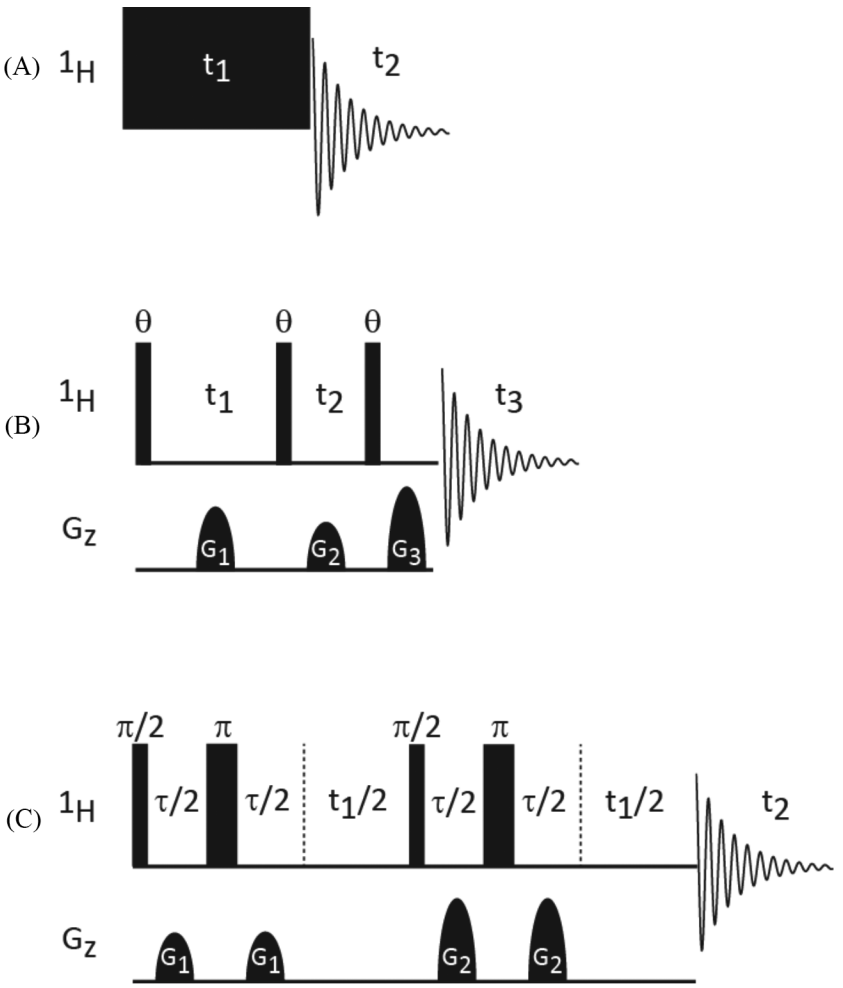

Fig. 3. Pulse sequences used in this study. Adjusting the rf pulse length in the rf nutation experiment in (A) to t_1 = 25 μs yields a typical one-dimensional ^{1}H spectra. The three-pulse stimulated-echo sequence in (B) is used to demonstrate the effect of rf inhomogeneity presented by the *open* coil geometry. The multiple spin echoes generated by this rf pulse sequence are selected with the pulsed field gradient values shown in table 1. The cross peak enhanced, pulsed field gradient filtered SECSY sequence in (C) is used to generate two-dimensional ^{1}H chemical-shift correlation spectra at elevated pressure.

Laboratory-specific Matlab software was written to skew the double Fourier-transformed SECSY data into two-dimensional chemical-shift-correlation spectra.

RESULTS AND DISCUSSION

To summarize the design changes, there are two simultaneous alterations that would allow geochemists to achieve higher pressures using the clamped-cell apparatus. The first of these is rotation of the coil to be coaxial with the sample tube, and the second is reconfiguration from the *closed* to *open* geometry. Spectral distortions related to these modifications are easily demonstrated and removed.

Open and Closed Geometries

The ^{1}H NMR spectra for the neat and diluted ethyl alcohol samples at two different pressures are shown in figure 4. These spectra were generated by fixing the

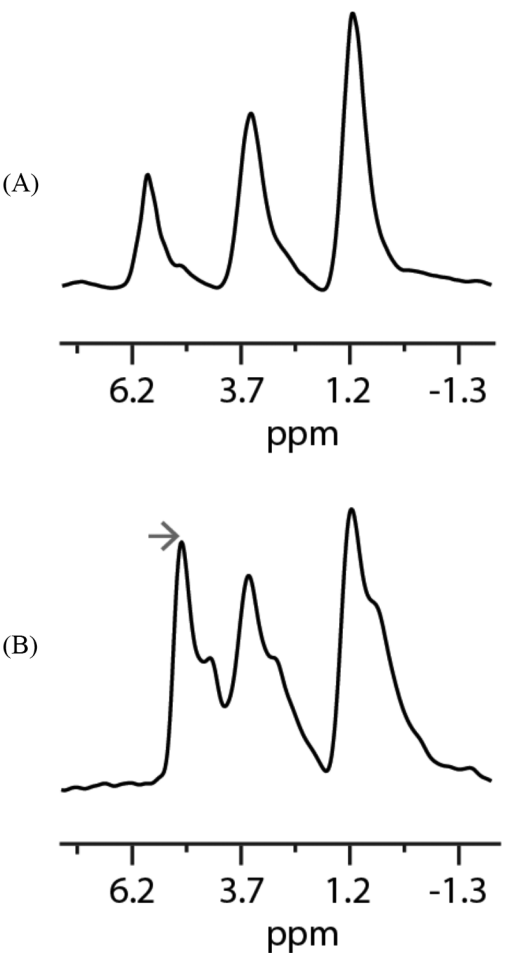

Fig. 4. One-dimensional ^{1}H NMR spectra for ethyl alcohol at 1.7 GPa in the *closed* geometry (A) and the 1:4 ethyl:methyl alcohol mixture at 2.8 GPa in the *open* geometry (B). The shoulders on the upfield side of the peaks in (B) are a shim artifact.

pulse length in the sequence shown in figure 3A to the standard $\pi/2$ rf pulse value. The spectrum for the pure ethyl alcohol sample at 1.7 GPa in the *closed* geometry that is shown in figure 4A displays three peaks centered at 1.2 ppm, 3.7 ppm, and 6.2 ppm peaks, respectively, that correspond to protons in the methyl, methylene, and hydroxyl groups in the ethyl alcohol molecule. The intensity and frequency of the 6.2 ppm peak changes from sample-to-sample, and with pressure up to the freezing pressure of the pure alcohol at $\approx$1.8 GPa. This spectral variation is undoubtedly due to chemical exchange between the ethyl alcohol hydroxyl proton and water. The sample-to-sample differences in the spectra are due to varying amounts of water mixing with the ethyl alcohol during storage and sample loading as no extreme precautions were taken to ensure that the ethyl alcohol remain dry. The pressure variation of the line position of the hydroxyl peak (near 6.2 ppm) is also expected because the equilibrium constant for proton exchange varies with pressure.

The ^{1}H NMR spectrum shown in figure 4B corresponds to the 1:4 ethyl:methyl alcohol sample at 2.8 GPa in the *open* configuration. This solution was used because

these pressures are well beyond the freezing point of either neat alcohol or aqueous solutions at ambient temperatures. The methyl group in ethyl alcohol again produces a resonance at 1.2 ppm but the 3.7 ppm methylene peak is less resolved from the ethyl alcohol hydroxyl, methyl alcohol hydroxyl, and water chemical exchange peak near 4.9 ppm. It is clear from the intensity of the hydroxyl/water peak, when compared to the methyl-group peak, that the as-received deuterated methyl alcohol contained some water. Moreover, the hydroxyl peak shifts by ≈1.3 ppm upon increasing pressure from 1.7 GPa in figure 4A to 2.8 GPa in figure 4B as indicated by the gray arrow in figure 4B.

The results shown in figure 4 indicate that high-resolution ^{1}H-NMR spectra can be collected from single-pulse experiments on liquids at GPa pressures. The ^{1}H NMR spectrum shown in figure 4B, which shows clearly resolved ^{1}H sites in ethyl alcohol, corresponds to the highest pressure liquids NMR data yet reported. This spectrum presents a 0.9 ppm peak resolution and was obtained without signal averaging. Although previous workers have conducted NMR experiments at higher pressures via the use of diamond-anvil cells (for example, Lee and others, 1987), these were on bulk materials and lacked the resolution necessary to do site-specific spectroscopy on individual compounds.

Although the *open* geometry produces more one-pulse NMR signal intensity than the *closed* configuration, the *open* geometry creates unwanted artifacts in multi-dimensional experiments. Specifically, the application of more than one rf pulse generates unwanted spin echoes in multi-pulse transient signals. These transient signals corrupt the useful coherence correlations following Fourier transformation of the signals. The origin of the problem lies in the *open* geometry itself — sample from outside of the rf coil contributes to the measured signal. In other words, from the point of view of pulse-sequence optimization, the *open* geometry suffers from severe rf inhomogeneity and introduces signal distortion.

These distortions are demonstrated by the Rabi-cycling transients shown in figure 5 that were generated by the nutation pulse sequence in figure 3A. In the nutation experiment, the integrated area of the NMR spectrum, or equivalently the amplitude of the time-domain signal at $t_2 = 0$, is tracked as a function of time, t_1, in figure 3A, which is also equivalent to an increased magnetization tip angle. In this way, the oscillation frequency and lifetime of the observed transient as a function of t_1, rf pulse length, or tip angle, respectively, yield information about the rf field strength and the field homogeneity offered by the particular solenoid NMR detection coil. A homogeneous field would yield an oscillating signal that decays exponentially with time, as shown in figure 5A.

The Rabi cycling transient shown in figure 5A corresponds to the *closed* configuration and displays exactly what one expects for a sample constrained to lie within the rf solenoid coil. The smooth damping of the signal reflects the high symmetry and homogeneity of the rf magnetic-flux lines threading through the length of the solenoid rf coil.

The signal becomes much more complicated when the sample is changed to the *open* geometry. Compare the Rabi cycling transient shown in figure 5B with that shown in figure 5A. In the *open* geometry, with no sample tube, the presence of sample inside and outside of the rf coil makes it impossible to invert the average signal. Essentially nuclei in different parts of the liquid sample experience different magnetization tip angles. For example, even if the center of the sample receives a perfect π-inversion pulse, the remainder of the sample, which is a relatively large volume, never inverts.

A comparison of figure 5A to figure 5B shows that changing the sample geometry to achieve higher pressures, from *closed* to *open*, also introduces field inhomogeneities. The inhomogeneous rf field in the *open* geometry introduces a complicated envelope function to the regular exponentially decreasing sinusoidal signal that is characteristic

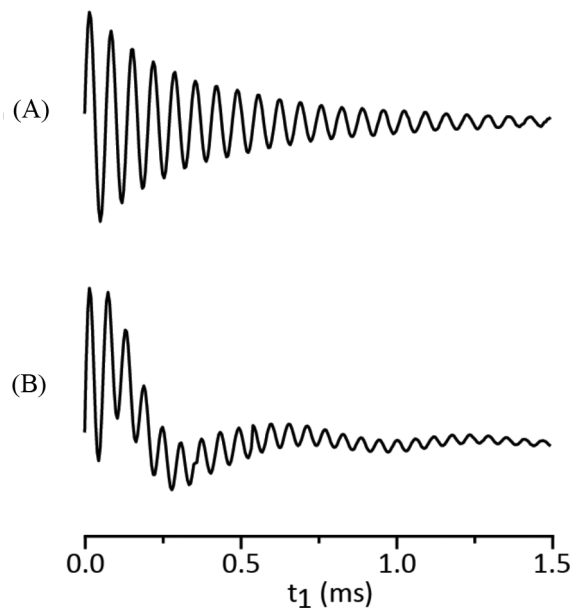

Fig. 5. Rabi cycling transients for the *closed* (A) and *open* (B) configurations. The $\nu_1 \approx 13$ kHz oscillation frequency and the first maximum at $t_1 = 1/4\nu_1 \approx 25$ μs yields the $\pi/2$ rf pulse time.

of the *closed* geometry, although the Rabi-cycling frequencies in the two cases appear similar. The similar Rabi frequencies are not surprising as the same rf power is being delivered to the two identically tuned rf circuits. The complicated envelope function created by the *open* geometry, which is a consequence of the inhomogeneous rf field and sample outside of the rf coil, presents problems when operating in multiple-pulse mode and must be corrected for high-pressure NMR using multiple pulses, as is demonstrated below.

Strategies to Eliminate Distortions

One problem for multiple-pulse operation is the meaning of a $\pi/2$ and π rf pulse in the *open* geometry. In the usual *closed* geometry, as displayed in figure 5A, a $\pi/2$ rf pulse tips the magnetization from the $+z$ equilibrium direction to the transverse plane and a π rf pulse inverts the magnetization. In the *open* geometry, a $\pi/2$ rf pulse corresponds to the rf pulse length that produces maximum signal while the π rf pulse is twice that length. Indeed, operation in this way always generates the maximum spin echo in the *open* configuration when the apparent $\pi/2$ pulse is followed a time τ later by the apparent π rf pulse.

Multiple-pulse NMR signal distortion can be demonstrated further with the three-pulse stimulated-echo pulse sequence shown in figure 3B. The transient signals following the application of three $\theta = \pi/2$ rf pulses with $t_1 = 83$ ms, and $t_2 = 18$ ms, as shown in the pulse sequence shown in figure 3B, to probes with the *closed* and *open* geometry in a poorly shimmed magnet, are shown in the first and second columns of figure 6A, respectively. Increasing the tip angle to $\theta = \pi$ yields the transient signals shown in the third and fourth columns of figure 6A for the *closed* and *open* configuration respectively. In the ideal *closed* geometry, four spin echoes are expected at the times t_2, $t_1 - t_2$, t_1, and $t_1 + t_2$ for three $\theta = \pi/2$ tip angle rf pulses, while no spin echoes are expected for three $\theta = \pi$ tip angle rf pulses.

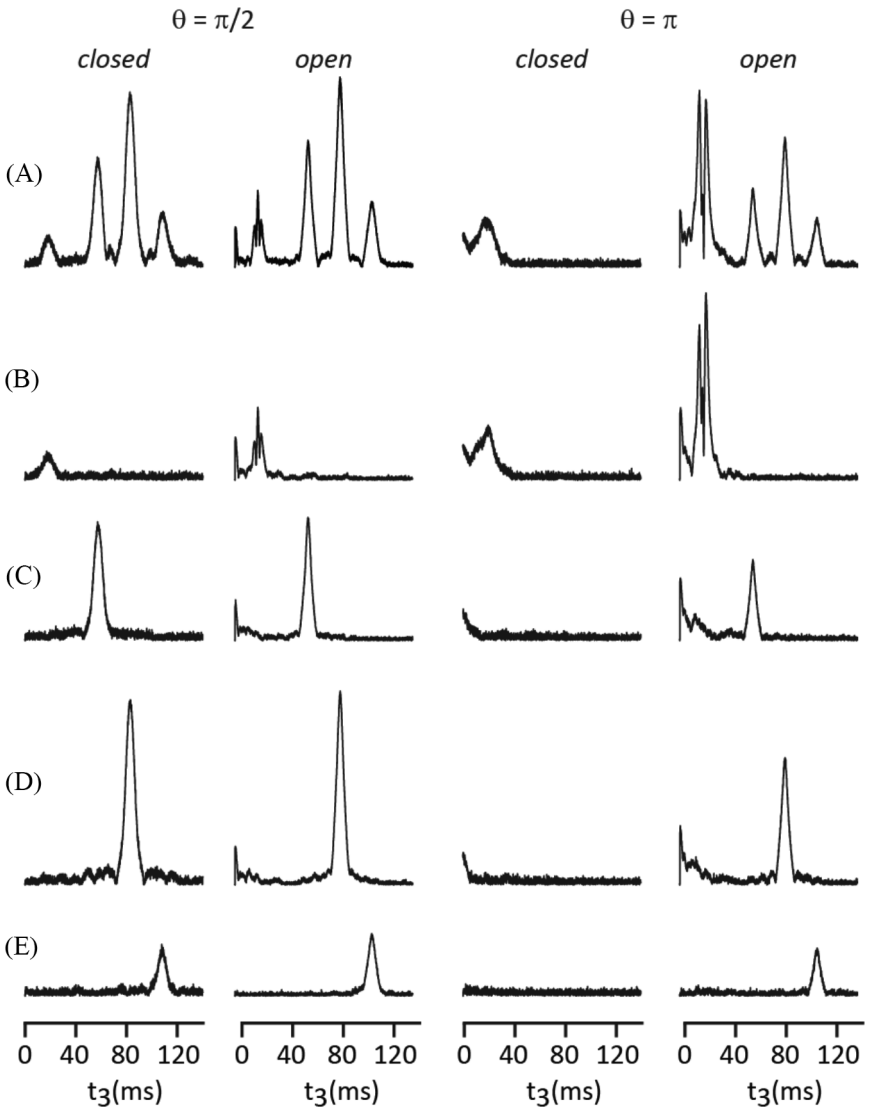

Fig. 6. Time-domain three-pulse stimulated echo transients generated from the pulse sequence shown in fig. 3B and the *closed* and *open* geometries in columns (1,3) and (2,4) when $\theta = \pi/2$ and π apparent tip angle pulses are used in columns (1,2) and (3,4). No pulsed field gradients are used in (A) while different ratios of the pulsed field gradient values according to table 1 used in the pulse sequence in fig. 3B generate the transients shown in (B) – (E).

It is clear from figure 6A that the results from applying three $\theta = \pi/2$ pulses to both geometries are consistent with expectations. However, the persistence of signal in the *open* configuration shown in the fourth column in figure 6A is not expected and is due to rf inhomogeneity and from the presence of sample outside of the solenoid rf coil. The persistence of signals like these would make correlation spectroscopy difficult and that will plague high-pressure NMR using the *open* coil orientation.

The presence of any signal for the application of three $\theta = \pi$ rf pulses to the *closed* configuration shown in the third column in figure 6A is initially surprising, but with

TABLE 1

Interpulse delay times and relative pulsed field gradient strengths used in the pulse sequence in figure 2 to select for echoes shown in figure 5

echo time in t_3	G_1†	G_2†	G_3†	row‡
t_2, t_1-t_2, t_1, t_1+t_2	0	0	0	(a)
t_2	1	0	0	(b)
t_1- t_2	1	1	0	(c)
t_1	0	1	0	(d)
t_1+ t_2	1	1	2	(e)

†A $G_n = 1$ value corresponds to a 3 G/cm, 3 ms long magnetic field gradient pulse.
‡The letters correspond to rows in figure 5.

reference to figure 5A, the effects of rf inhomogeneity reveal themselves in the form of damping after one signal-oscillation period. Consequently, one does expect some small residual signal due to slightly inhomogeneous rf in the *closed* geometry, but not the large signal shown in the fourth column in figure 5A for the *open* configuration. All of the transients shown in figure 6 correspond to just a single acquisition, suggesting that simple phase cycling can be used to remove this small parasitic signal.

The problem restated is that any pair of rf pulses in a multiple-pulse sequence can lead to signal refocusing that corrupts the desired transient signal. One solution to this rf-inhomogeneity problem is to employ pulsed magnetic-field gradients to edit the measured transients and to remove these unwanted spin echoes. Table 1 shows relative values for pulsed-field-gradient strengths that can be used in the stimulated-echo pulse sequence in figure 3B to select any individual spin echo. A value of $G_n = 1$ corresponds to the application of a 3 G/cm, 3-ms-long field gradient pulse and higher values of G_n linearly scale the amplitude. The letters in the far right column in table 1 pertain to the labels in figure 6. For example, application of $G_1 = G_2 = G_3 = 0$ from the first row of table 1 yields the responses shown in figure 6A while $G_1 = G_2 = 1$ and $G_3 = 2$ from the last row of table 1 produces the transients shown in figure 6E. The selection of any single echo using pulsed magnetic-field gradients, even in the presence of severe rf inhomogeneity in the *open* geometry in the far right column in figure 6, suggests that existing multiple pulse sequences can be modified for use when the rf coil is immersed in the sample, which considerably facilitates NMR for GPa pressures.

The nutation- and stimulated-echo results in figures 5 and 6 demonstrate that artifacts developed from having sample outside of the rf coil must be corrected when using the *open* geometry. The magnetic field was poorly shimmed and left inhomogeneous in order to resolve the multiple spin echoes that are shown in figure 6. In the case of the apparently well-shimmed magnet that produces the chemical-shift-resolved ^{1}H NMR spectra in figure 4, the ≈50 Hz wide peaks are due to static field inhomogeneity as $T_1 \approx T_2 \approx 1$ s for the mixture that produces the spectrum shown in figure 4B. Although the static field is much better in figure 4 than in figure 6, significant signal attenuation and unwanted spin echoes will occur in multiple pulse experiments where chemical-shift correlations are desired as pulse delays on the order of $1/2J \approx 100$ ms for a ^{1}H – ^{1}H scalar coupling of $J \approx 5$ Hz are required.

There is a pulse sequence that can be used to compensate for the rf- and static field inhomogeneity in the *open* geometry that is useful in high-pressure NMR. The sequence is spin-echo correlated spectroscopy, known as the SECSY experiment, and was pioneered by Wüthrich and Ernst (Nagayama and others, 1979, 1980) and championed by Hall and Norwood (1987). Unfortunately the static-field homogeneity for the high-pressure probe is still too poor to achieve any substantial cross-peak intensity upon application of the simple two $\pi/2$ rf pulse SECSY pulse sequence. The failure is because the inhomogeneous static magnetic field damps the transient signal in the indirectly detected t_1 dimension before components of the signal that reflect nuclear-spin coupling develop. This damping significantly reduces the cross-peak intensity, which is essential for usefulness of the method.

In an attempt to resolve this problem, two π rf pulses are added to the basic two $\pi/2$ rf pulse SECSY experiment, as illustrated in figure 3C. The first π rf pulse is used to generate a maximum antiphase magnetization and signal refocusing at the time, 2τ, after the first $\pi/2$ rf pulse. The standard indirect delay of $t_1/2$ occurs before the second $\pi/2$ rf pulse. The second π rf pulse is used to rephase the earlier 2τ-encoded antiphase magnetization. Detection commences $t_1/2$ later at the top of the spin echo. The added π rf pulses allow the nuclear-spin-coupling-dependent signal components to develop (J evolution), ultimately enhancing cross-peak intensity.

This enhancement is, however, not entirely beneficial, as demonstrated in figure 6. These added rf pulses also generate unwanted spin echoes when applied to the *open* geometry. It is for this reason that the two pairs of 3-ms-long pulsed-magnetic-field gradients were included in the pulse sequence shown in figure 3C. These magnetic-field-gradient pulses guarantee that any measured signal is transverse throughout the entire duration of the sequence. Thus any effects of inhomogeneous rf due to magnetization remaining, or being stored along, the z axis are eliminated.

^{1}H-^{1}H NMR Spectra at Gigapascal Pressures

The key point is that these pulse-sequence adaptations allow a ^{1}H-^{1}H NMR spectrum to be measured for liquids at GPa pressures. The two-dimensional correlation spectra shown in figure 7 result after applying a skew transformation to the double Fourier-transformed SECSY transients acquired using the pulse sequence in figure 3C. The 1.4 GPa spectrum for ethyl alcohol in figure 7A displays the expected cross peak between the 1.2 ppm resonance for the methyl-group protons and the 3.7 ppm resonance for the methylene-group protons. There are no cross peaks to the hydroxyl resonance that is chemically exchanging with water. A similar set of cross peaks is generated at higher 2.8 GPa for the 1:4 ethyl:methyl alcohol mixture as shown in figure 7B. The methylene autocorrelated peak at 3.7 ppm in this mixture is below the displayed contour levels because the intensity added to the cross peak corresponds to a decreased intensity of the autocorrelated peak. The results shown in this figure at 2.8 GPa are, to our understanding, the highest pressure two-dimensional NMR spectrum yet reported and promise similar results for aqueous solutions once temperatures can be increased to prevent pressure-induced freezing.

CONCLUSIONS

The essential result of this study is that solution NMR spectroscopy should be achievable for geochemists on aqueous solutions to pressure ranges that approach the limit of the HKF model, at least at relatively low temperatures. Here is described an NMR probe that produces chemical-shift-resolved ^{1}H-^{1}H NMR correlation spectra for solutions at pressures of 2.8 GPa, and beyond. The ultimate pressures that can be achieved with this design probably lie in the 3.5 to 4.0 GPa range (Walker, 1999; Uwatoko and others, 2002), although there are several barriers remaining to be addressed.

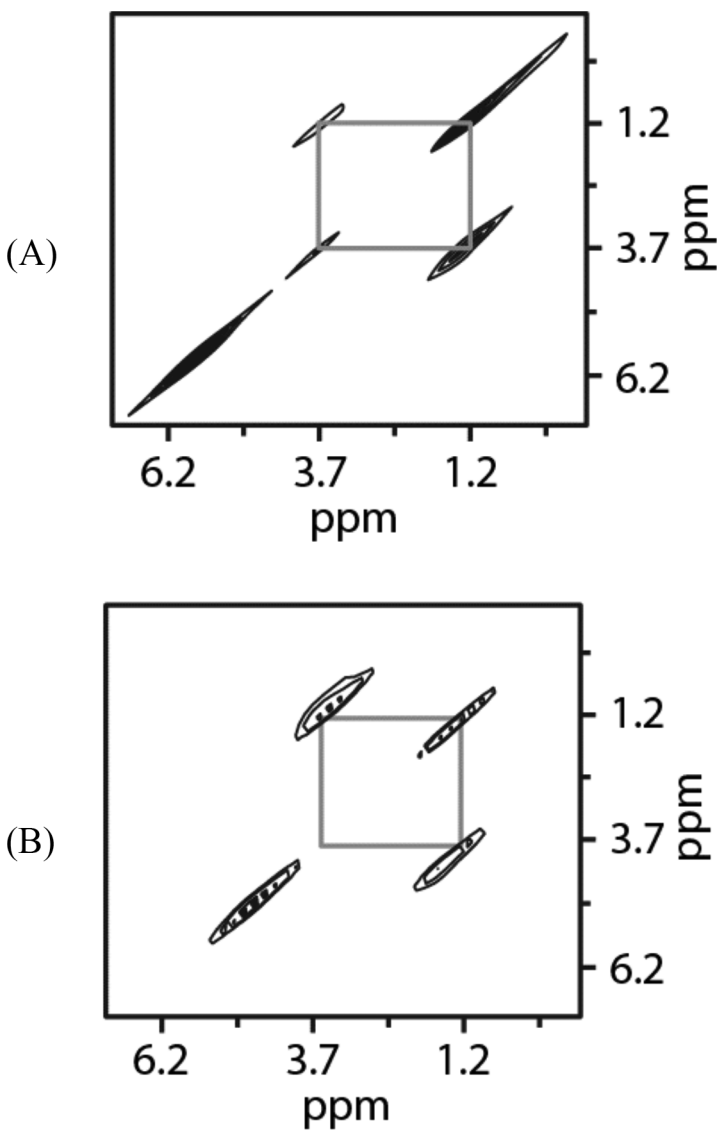

Fig. 7. Two-dimensional chemical-shift correlation spectra for ethyl alcohol at 0.4 GPa in the *closed* geometry in (A) and for the 1:4 ethyl:methyl alcohol mixture at 2.8 GPa in the *open* configuration in (B). The 3.7 ppm autocorrelated peak in (B) is below the displayed contour levels.

The first and obvious barrier is temperature. Water freezes at ≈0.9 GPa at ambient temperatures, although the range can be extended by salt addition (Ochoa and others, 2016) and many organic pressure-transmission oils also freeze at low pressure (Yokogawa and others, 2007; Murata and others, 2008). Designs that work at both elevated pressures and elevated temperatures are essential to make this spectroscopy useful to geochemists and are now being investigated.

The strength of the nonmagnetic materials and the integrity of the feedthroughs and wires in the circuit also may limit the ultimate pressures. If the ultimate pressures are limited only by the strength of the cylinder materials, the key parameter is the ratio

of outer diameter of the confining cylinder to the diameter of the inner piston. In previous experiments (Pautler and others, 2014; Ochoa and others, 2015, 2016), these diameters were 25.4 mm and 6.35 mm, respectively, yielding a ratio of ≈4.0. This ratio is adequate for experiments up to ≈2.0 GPa using Berylco-25. Burst-strength calculations suggest that this range could be extended to ≈3.0 GPa if the diameter ratio is increased from 4.0 to 6.3, and by fabricating the cylinder from a stronger nonmagnetic alloy. One such material is the MP35N alloy used to generate the results shown in figures 2, 4 and 7, and which has an ultimate yield strength higher than Berylco-25. Pressures greater than 4.0 GPa have been achieved by using the exotic NiCrAl 40HNU-VI alloy (Walker, 1999; Uwatako and others, 2002), which only recently became available in the United States (Carmichael, ms, 2015). This 40HNU-VI alloy is particularly important because the ultimate yield strength is 2.0 to 2.1 GPa at ambient temperatures, which is higher than MP35N (1.84 GPa). The 40HNU-VI alloy is also nonmagnetic and retains much of its strength (~1.7 GPa) to 500 °C (see Walker, 2005 and Fig. 10 in Carmichael, ms, 2015).

ACKNOWLEDGMENTS

The authors thank Professors Rudi van Eldik and James Kirkpatrick for perceptive and helpful reviews. We also thank Professor Keizo Murata of Osaka City University for advice about nonfreezing pressure fluids. The authors also thank Mr. Justin Carmichael, Mr. Brian Devine and Dr. Larry Anovitz for advice about the 40HNU-VI alloy, and Peter Klavins for help with the calibration curve. This work is supported by the Department of Energy Office of Basic Energy Sciences via grant DE-FG02-05ER15693.

REFERENCES

Asano, T., and Le Noble, W. J., 1978, Activation and reaction volumes in solution: Chemical Reviews, v. 78, n. 4, p. 407–489, https://doi.org/10.1021/cr60314a004

Ballard, L., Yu, A., Reiner, C., and Jonas, J., 1998, A high-pressure, high-resolution NMR probe for experiments at 500 MHz: Journal of Magnetic Resonance, v. 133, n. 1, p. 190–193, https://doi.org/10.1006/jmre.1998.1463

Carmichael, J. R., ms, 2015, A high-pressure cell for spark-plasma sintering: Knoxville, Tennessee, University of Tennessee, Master's Thesis, 54 p., http://trace.tennessee.edu/utk_gradthes/3441

De Langen, M., and Prins, K., 1995, NMR probe for high pressure and high temperature: Review of Scientific Instruments, v. 66, n. 11, p. 5218–5221, https://doi.org/10.1063/1.1146087

Dewaele, A., Torrent, M., Loubeyre, P., and Mezouar, M., 2008, Compression curves of transition metals in the Mbar range: Experiments and projector augmented-wave calculations: Physical Review B, v. 78, n. 10, p. 1–13, https://doi.org/10.1103/PhysRevB.78.104102

Drljaca, C., Hubbard, C. D., Van Eldik, R., Asano, T., Basilevsky, M. V., and Le Noble, W. J., 1998, Activation and reaction volumes in solution. 3: Chemical Reviews, v. 98, n. 6, p. 2167–2289, https://doi.org/10.1021/cr970461b

Facq, S., Daniel, I., Montagnac, G., Cardon, H., and Sverjensky, D. A., 2014, *In situ* Raman study and thermodynamic model of aqueous carbonate speciation in equilibrium with aragonite under subduction zone conditions: Geochimica et Cosmochimica Acta, v. 132, p. 375–390, https://doi.org/10.1016/j.gca.2014.01.030

——— 2016, Carbon speciation in saline solutions in equilibrium with aragonite at high pressure: Chemical Geology, v. 431, p. 44–53, https://doi.org/10.1016/j.chemgeo.2016.03.021

Hall, L. D., and Norwood, T. J., 1987, Measurement of high-resolution NMR spectra in an inhomogeneous magnetic field: Journal of the American Chemical Society, v. 109, n. 24, p. 7579–7581, https://doi.org/10.1021/ja00258a080

Jonas, J., 1980, Nuclear magnetic resonance studies at high pressures: Reviews of Physical Chemistry of Japan, v. 50, p. 19–35.

Koyama-Nakazawa, K., Koeda, M., Hedo, M., and Uwatoko, Y., 2007, *In situ* pressure calibration for piston cylinder cells via ruby fluorescence with fiber optics: Review of Scientific Instruments, v. 78, p. 1–3, https://doi.org/10.1063/1.2749451

Lang, E. W., and Lüdemann, H. D., 1993, Density dependence of rotational and translational molecular dynamics in liquids studied by high pressure NMR: Progress in Nuclear Magnetic Resonance Spectroscopy, v. 25, n. 6, p. 507–633, https://doi.org/10.1016/0079-6565(93)80007-G

Lee, S.-H., Luszczynski, K., Norberg, R. E., and Conradi, M. S., 1987, NMR in a diamond anvil cell: Review of Scientific Instruments, v. 58, p. 415–417, https://doi.org/10.1063/1.1139246

Mao, H. K., Xu, J., and Bell, P. M, 1986, Calibration of the ruby pressure gauge to 800 kbar under

quasi-hydrostatic conditions: Journal of Geophysical Research-Solid Earth, v. 91, n. B5, p. 4673–4676, https://doi.org/10.1029/JB091iB05p04673

Meier, T., Reichardt, S., and Haase, J., 2015, High-sensitivity NMR beyond 200,000 atmospheres of pressure: Journal of Magnetic Resonance, v. 257, p. 39–44, https://doi.org/10.1016/j.jmr.2015.05.007

Murata, K., Yokogawa, K., Yoshino, H., Klotz, S., Munsch, P., Irizawa, A., Nishiyama, M., Iizuka, K., Nanba, T., Okada, T., Shiraga, Y., and Aoyama, S., 2008, Pressure transmitting medium Daphne 7474 solidifying at 3.7 GPa at room temperature: Review of Scientific Instruments, v. 79, n. 8, p. 1–7, https://doi.org/10.1063/1.2964117

Nagayama, K., Wüthrich, K., and Ernst, R. R., 1979, Two-dimensional spin echo correlated spectroscopy (SECSY) for ^{1}H NMR studies of biological macromolecules: Biochemical and Biophysical Research Communications, v. 90, n. 1, p. 305–311, https://doi.org/10.1016/0006-291X(79)91625-5

Nagayama, K., Kumar, A., Wüthrich, K., and Ernst, R. R., 1980, Experimental techniques of two-dimensional correlated spectroscopy: Journal of Magnetic Resonance, v. 40, n. 2, p. 321–334, https://doi.org/10.1016/0022-2364(80)90255-3

Ochoa, G., Pilgrim, C. D., Martin, M. N., Colla, C. A., Klavins, P., Augustine, M. P., and Casey, W. H., 2015, ^{1}H and ^{139}La NMR spectroscopy in aqueous solutions at geochemical pressures: Angewandte Chemie International Edition, v. 127, n. 51, p. 15664–15667, https://doi.org/10.1002/ange.201507773

Ochoa, G., Colla, C. A., Klavins, P., Augustine, M. A., and Casey, W. H., 2016, NMR spectroscopy of some electrolyte solutions to 1.9 GPa: Geochimica et Cosmochimica Acta, v. 193, p. 66–74, https://doi.org/10.1016/j.gca.2016.08.013

Pan, D., Spanu, L., Harrison, B., Sverjensky, D. A., and Galli, G., 2013, Dielectric properties of water under extreme conditions and transport of carbonates in the deep Earth: Proceedings of the National Academy of Sciences of the United States of America, v. 110, n. 17, p. 6646–6650, https://doi.org/10.1073/pnas.1221581110

Pautler, B. G., Colla, C. A., Johnson, R. L., Klavins, P., Harley, S. J., Ohlin, C. A., Sverjensky, D. A., Walton, J. H., and Casey, W. H., 2014, A high-pressure NMR probe for aqueous geochemistry: Angewandte Chemie International Edition, v. 53, n. 37, p. 9788–9791, https://doi.org/10.1002/anie.201404994

Piermarini, G. J., Block, S., and Barnett, J. D., 1973, Hydrostatic limits in liquids and solids to 100 kbar: Journal of Applied Physics, v. 44, p. 5377–5382, https://doi.org/10.1063/1.1662159

Sverjensky, D. A., and Huang, F., 2015, Diamond formation due to a pH drop during fluid-rock interactions: Nature Communications, v. 53, p. 1689–1699, https://doi.org/10.1038/ncomms9702

Sverjensky, D. A., Harrison, B., and Azzolini, D., 2014, Water in the deep Earth: The dielectric constant and the solubilities of quartz and corundum to 60 kbar and 1200 °C: Geochimica et Cosmochimica Acta, v. 129, p. 125–145, https://doi.org/10.1016/j.gca.2013.12.019

Uwatoko, Y., Todo, S., Ueda, K., Uchida, A., Kosaka, M., Mori, N., and Matsumoto, T., 2002, Material properties of Ni-Cr-Al alloy and design of a 4 GPa class non-magnetic high-pressure cell: Journal of Physics Condensed Matter, v. 14, n. 44, p. 11291–11296, https://doi.org/10.1088/0953-8984/14/44/469

Van Eldik, R., Asano, T., and Le Noble, W. J., 1989, Activation and reaction volumes in solution. 2: Chemical Reviews, v. 89, n. 3, p. 549–688, https://doi.org/10.1021/cr00093a005

Walker, I. R., 1999, Nonmagnetic piston-cylinder pressure cell for use at 35 kbar and above: Review of Scientific Instruments, v. 70, p. 3402–3412, https://doi.org/10.1063/1.1149927

——— 2005, Considerations on the selection of alloys for use in pressure cells at low temperatures: Cryogenics, v. 45, n. 2, p. 87–108, https://doi.org/10.1016/j.cryogenics.2004.05.002

Wasserman, E., Wood, B., and Davies, A., 1995, Equation of state for aqueous silica species at pressures from 1 bar to 20 kbar and temperatures from 25° to 900 °C based on simulated values of the dielectric constant: Chemical Geology, v. 121, n. 1–4, p. 3–9, https://doi.org/10.1016/0009-2541(94)00157-4

Yokogawa, K., Murata, K., Yoshino, H., and Aoyama, S., 2007, Solidification of high-pressure medium Daphne 7373: Japanese Journal of Applied Physics, v. 46, Part 1, n. 6A, p. 3636–3639, https://doi.org/10.1143/JJAP.46.3636